

Spatial resolution measurement for iterative reconstruction by use of image-averaging techniques in computed tomography

Atsushi Urikura · Katsuhiko Ichikawa ·
Takanori Hara · Eiji Nishimaru · Yoshihiro Nakaya

Received: 12 February 2014/Revised: 19 May 2014/Accepted: 20 May 2014/Published online: 1 June 2014
© Japanese Society of Radiological Technology and Japan Society of Medical Physics 2014

Abstract The purpose of our study was to investigate the validity of a spatial resolution measuring method that uses a combination of a bar-pattern phantom and an image-averaging technique, and to evaluate the spatial resolution property of iterative reconstruction (IR) images with middle-contrast (50 HU) objects. We used computed tomography (CT) images of the bar-pattern phantom reconstructed by the IR technology Adaptive Iterative Dose Reduction 3D (AIDR 3D), which was installed in the multidetector CT system Aquilion ONE (Toshiba Medical Systems, Otawara, Japan). The contrast of the bar-pattern image was set to 50 HU, which is considered to be a middle contrast that requires higher spatial resolution clinically. We employed an image-averaging technique to eliminate the influence of image noise, and we obtained

averaged images of the bar-pattern phantom with sufficiently low noise. Modulation transfer functions (MTFs) were measured from the images. The conventional wire method was also used for comparison; in this method, AIDR 3D showed MTF values equivalent to those of filtered back projection. For the middle-contrast condition, the results showed that the MTF of AIDR 3D decreased with the strength of IR processing. Further, the MTF of AIDR 3D decreased with dose reduction. The image-averaging technique used was effective for correct evaluation of the spatial resolution for middle-contrast objects in IR images. The results obtained by our method clarified that the resolution preservation of AIDR 3D was not sufficient for middle-contrast objects.

Keywords Computed tomography · Iterative reconstruction · Spatial resolution · Image noise · Dose reduction · MTF

A. Urikura (✉) · Y. Nakaya
Department of Diagnostic Radiology, Shizuoka Cancer Center,
1007 Shimonagakubo, Nagaizumi, Sunto, Shizuoka 411-8777,
Japan
e-mail: at.urikura@scchr.jp

A. Urikura
Graduate School of Medical Science, Kanazawa University,
5-11-80 Kodatsuno, Kanazawa, Ishikawa 920-0942, Japan

K. Ichikawa
Institute of Medical, Pharmaceutical and Health Sciences,
Kanazawa University, 5-11-80 Kodatsuno, Kanazawa,
Ishikawa 920-0942, Japan

T. Hara
Department of Medical Technology, Nakatsugawa Municipal
General Hospital, 1522-1 Komanba, Nakatsugawa,
Gifu 508-0011, Japan

E. Nishimaru
Department of Radiology, Hiroshima University Hospital,
1-2-3 Kasumi, Minami-ku, Hiroshima 734-8551, Japan

1 Introduction

Multidetector computed tomography (MDCT) has played an important role in diagnostic imaging; it is increasingly being used because it can quickly and accurately help diagnose various diseases [1–3]. However, the increase in CT examinations prompts the need for a discussion of radiation risks versus medical benefits [4]. For reducing the risk of CT examination, a number of dose reduction techniques have been developed and installed in clinical MDCT systems [5].

In the image reconstruction method of CT, filtered back projection (FBP) has been the gold standard for several decades. Recently, some reconstruction methods that make use of the iterative reconstruction (IR) technique have been

developed by major CT manufacturers, and these methods have been applied to clinical CT examinations [6–8].

IRs are used for reducing the radiation dose because they have features that reduce the image noise occurring mainly due to radiation quantum fluctuation while maintaining the spatial resolution. Because most IRs are designed on the basis of non-linear processes [9, 10], their image properties are complicated in comparison with those of FBP, and the image quality evaluation methods for IR images have not yet been established. The conventional methods for spatial resolution, noise, and slice thickness cannot be applied because they were devised for images reconstructed by FBP with a linear signal response.

The resolution property is important for the evaluation of image quality in CT, and high-contrast objects such as metal wires and high-contrast periodic patterns are required for obtaining accurate results with the conventional measurement method [11]. Although there are some reports regarding the image quality of IRs, in which the resolution properties were evaluated with high-contrast objects [6, 7, 9, 12], the results represent resolution properties only for high-contrast parts of the human body (e.g., bones) and do not indicate the properties for low- or middle-contrast objects.

In general, spatial resolution is not important for detection of low-contrast objects. This is apparent because objects with diameters smaller than 2.0 mm are not included in low-contrast resolution phantoms [13]. Liver tumors, which had been reported as having 5–20 Hounsfield units (HU) in contrast with normal liver parenchyma [14, 15], are well-known as typical low-contrast objects in clinical CT images. Therefore, the evaluation of spatial resolution is less important in such low-contrast regions. On the other hand, for diagnosis of lipid-rich plaque (with an attenuation of about 50 HU) in coronary CT, representing a detailed structure of the plaques is important [16]. Deep venous thrombosis with 50 HU contrast also requires higher resolution for accurate diagnosis [17]. Therefore, it is important to evaluate the spatial resolution of objects with contrasts of around 50 HU (middle contrast) for assessing the resolution property of IRs.

Richard et al. [18] demonstrated the measurement method for the modulation transfer function (MTF) with averaging of the edge spread functions obtained from the circular objects built in the ACR phantom (model 464, Gammex, WI). They revealed that MTFs obtained from adaptive statistical iterative reconstruction (ASIR, GE, WI) and model-based iterative reconstruction depends on the contrast and the exposure dose. In their study, the circular objects with contrasts of 995, 120, and 95 HU were used for MTF measurement, and remarkable deviations of MTF values (error bars) due to image noise were shown in MTF results for objects with contrasts of 120 and 95 HU.

Therefore, it is suspected that the deviation becomes larger for the middle contrast due to its lower contrast-to-noise ratio, and it is not clear that their method can be applied to such middle-contrast objects.

Our purpose in this study was to investigate the validity of our proposed MTF measurement method, which can be applied to middle-contrast (50 HU) objects, and to evaluate the spatial resolution differences between FBP and IR images.

2 Methods and materials

2.1 CT scanner and iterative reconstruction

All examinations were performed with a multidetector CT scanner (Aquilion ONE; Toshiba Medical Systems, Otawara, Japan). This system was equipped with 320-row detector arrays that could obtain up to 160-mm coverage in the z -direction. We evaluated an IR technology, Adaptive Iterative Dose Reduction 3D (AIDR 3D) which was installed in Aquilion ONE. To reduce the image noise, AIDR 3D uses an algorithm to work in both the raw data and image data domains, while spatial resolution and structural edges are preserved and even improved [9]. In addition, AIDR 3D has four strengths of noise reduction levels (weak, mild, standard, and strong). All data acquisitions were performed with a non-helical scan mode, which was used routinely for coronary CT angiography and brain CT examinations.

2.2 Bar-pattern method

An acrylic bar-pattern phantom as shown in Fig. 1a was used. This phantom consisted of six bar-pattern segments with bar sizes of 0.5–5.0 mm (corresponding frequencies, 1.0–0.1 cycles/mm), and the CT number was 135 HU for the CT system used. The bar-pattern phantom was fixed in a cylindrical acrylic case with a diameter of 200 mm, so that the surface plane of the bar-pattern phantom was parallel to the axial plane of the cylindrical case, as shown in Fig. 1b. The cylindrical case was placed at the isocenter, and the phantom rotation was adjusted so that the long axis of the bar-pattern phantom was tilted slightly (roughly 2.5°) relative to the y -axis. This tilting was needed to provide a sufficiently small effective sampling pitch for the Fourier analysis described below [19]. To make the contrast (Δ HU) between the bar pattern and the background 50 HU, the case was filled with diluted iodine contrast medium (2.7 mgI/ml). For setting of the high-contrast conditions that were used for the validity investigation described in Sect. 2.5, the case was filled with air (Δ HU = 1,135 HU).

Fig. 1 **a** Acrylic bar-pattern phantom used in this study. Thickness of the phantom was 5.0 mm. **b** The bar-pattern phantom was placed in a cylindrical acrylic case with a diameter of 200 mm

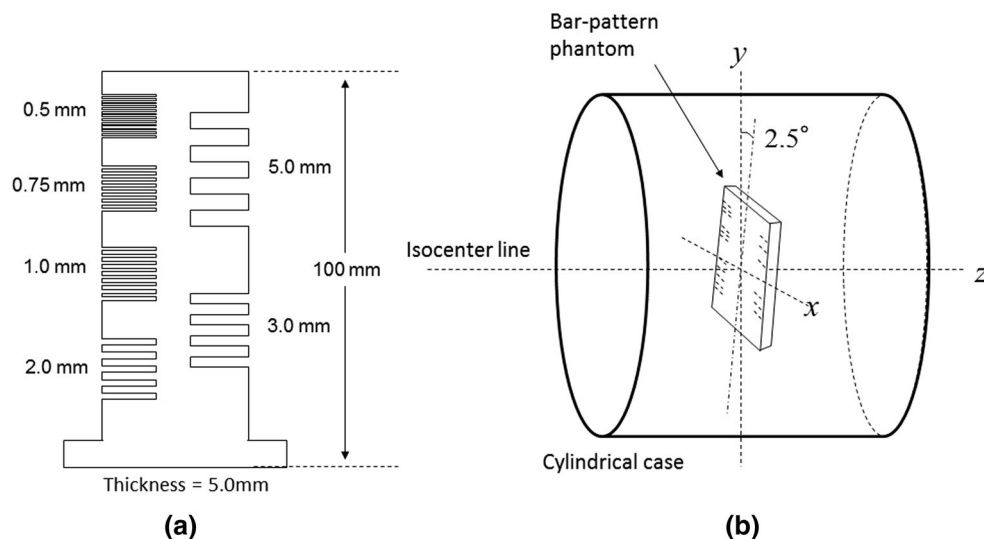
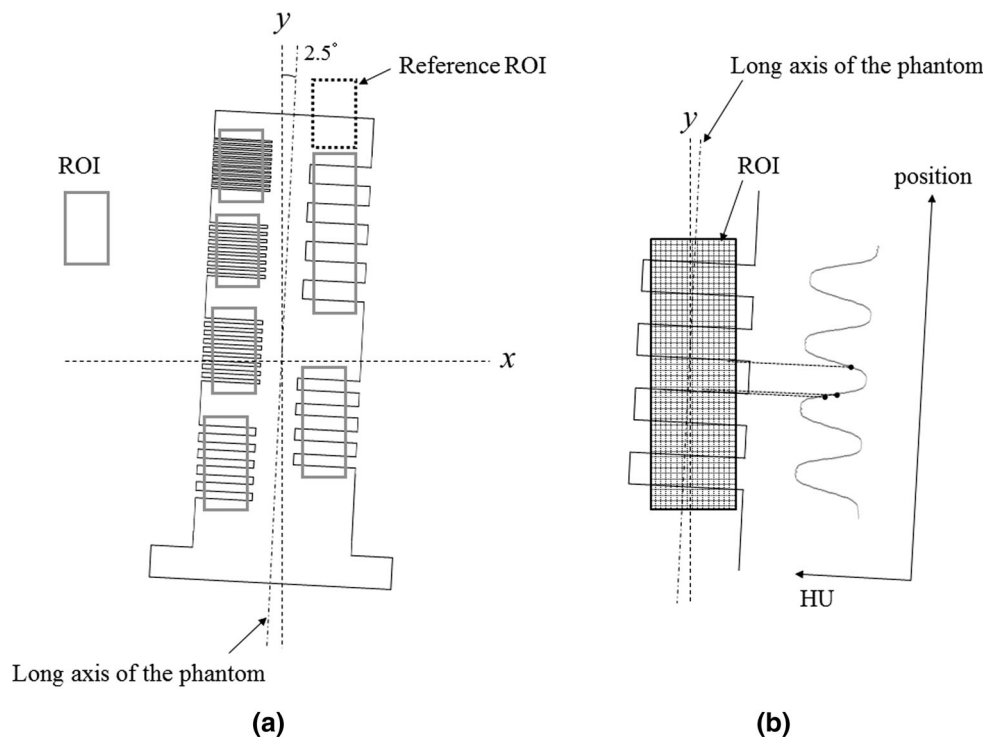


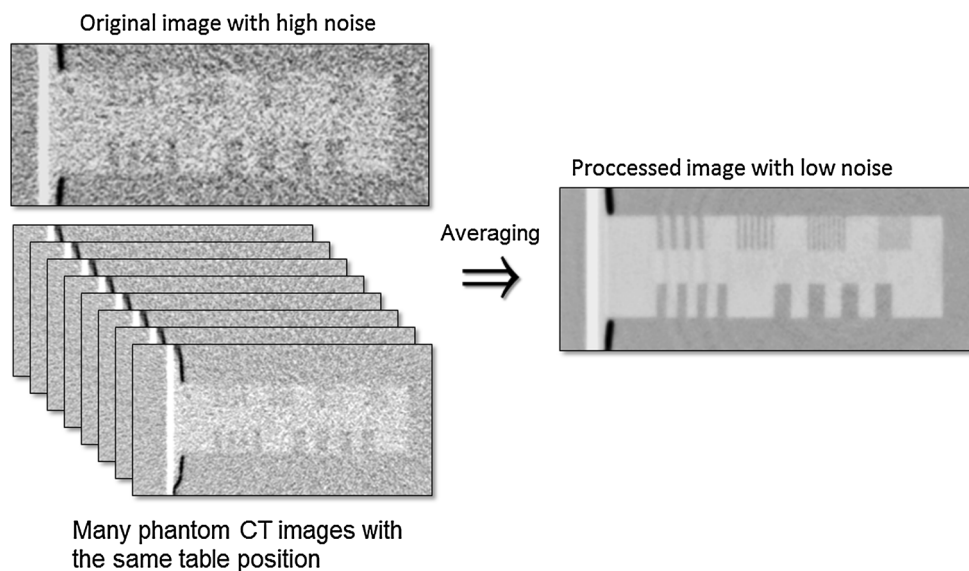
Fig. 2 **a** Placement of regions of interest in a bar-pattern phantom image. The reference region of interest was used to determine the input sinusoidal amplitude A_0 . **b** Within the ROI, various pixel values were projected onto a line orthogonal to the bar line



MTFs were measured by a method employing the Fourier transform for extracting sinusoidal amplitudes from square-wave profiles across each bar-pattern segment [20]. For MTF calculations, the following steps were performed: (1) Rectangular regions of interest (ROIs) were placed at each segment, as shown in Fig. 2a. (2) Within each ROI, various pixel values were projected onto a line orthogonal to the bar line, and we obtained the response for a square-wave profile with a finer effective sampling pitch than the actual pixel pitch (Fig. 2b). The projection angle was finely adjusted around 2.5° so that the blurring of projected data due to misalignment was visually minimum. This

procedure provides an oversampled profile and therefore allows measurement of the frequency response of the segment beyond the Nyquist limit. (3) By application of the Fourier transform to the profile obtained, the sinusoidal amplitude (A_n , n = segment number) for a fundamental frequency in the profile was extracted. (4) The input amplitude (A_0) was determined by the contrast measured from the reference ROI which was located in the near-top region of the phantom, as shown in Fig. 2. (5) The MTF value at each segment (frequency) was obtained by calculation of the ratio of the amplitudes from A_n to A_0 . The slight effect of the binning process used in the step (2) was

Fig. 3 Overview of the image-averaging technique. For obtaining several images with the same table position, the phantom was scanned 50 times with the table in a fixed position



corrected by the sinc function corresponding to a width of the bin [21].

The scanning conditions were 120 kV, 80 mA, 2.0 s/rot., and 80×0.5 mm detector configuration. The CT images were reconstructed by FBP and AIDR 3D with a 240-mm display field of view (DFOV), a 0.5-mm slice thickness, and a reconstruction kernel of FC12.

For the middle-contrast condition, we scanned the phantom and then selected two axial images including axial planes of the bar-pattern phantom from the reconstructed images. The scanning was repeated 50 times, and consequently, 100 images were obtained for each FBP and two strengths of AIDR 3D (weak and strong). These images were used for investigations in which we used the image-averaging technique we adopted to measure the correct resolution properties, as described in the subsequent sections. For the high-contrast condition, we performed the phantom scanning two times, and four images were obtained for each reconstruction.

2.3 Image-averaging technique

The spatial resolution in CT images needs to be evaluated in a noiseless field [11]. To satisfy this requirement in conventional spatial resolution measurements, a high-contrast object (e.g., metal wire) is used, which can approximate the noiseless condition. Therefore, middle- or low-contrast objects cannot be used for the measurement because the noise requirements are not satisfied on such contrasts. To solve this problem, we used an image-averaging technique which reduces image noise by averaging many images at the same table position. By application of this technique, quantum noise, which is well-known as a dominant random noise component in CT image noise, can

be reduced, and therefore we were able to obtain bar-pattern low-noise images suitable for resolution measurement (Fig. 3). This procedure rendered unnecessary the use of approximation techniques such as data fitting. To obtain many images with the same table position, we repeated the phantom scanning several times at a fixed table position.

2.4 Required contrast-to-noise ratio

We investigated the minimally required contrast-to-noise ratio (CNR) [22] for obtaining a correct resolution measurement using the bar-pattern phantom. Specifically, we used the FBP images of the bar-pattern phantom in this investigation, and CT images with various CNRs were obtained by adjustment of the image number of the averaging technique. For correct assessment of the resolution property, it was important that the square-wave profile was obtained correctly at each ROI. Thus, we adopted a contrast transfer factor (CTF) to evaluate the precision of the profile because the MTF error is expected to be at about the same level as the CTF error. In each averaged image, a CTF for each bar-pattern segment with a square-wave frequency of u was calculated by the following equation.

$$\text{CTF}(u) = \text{Contrast}_{\text{target}} / \text{Contrast}_{\text{reference}} \quad (1)$$

$\text{Contrast}_{\text{reference}}$ and $\text{Contrast}_{\text{target}}$, respectively, were differences between the upper and lower levels of the profiles obtained in the reference ROI and an ROI at each bar-pattern segment shown in Fig. 2. The upper and lower levels were calculated by averaging of several points at the upper and lower peaks, respectively.

We tested the following five CNR levels: 20, 24, 28, 32, and 36; their corresponding image numbers for the averaging were 44, 60, 100, 140 and 180, respectively. The

CTF values measured from the averaged images were compared with the true CTF values, which were defined as those measured from an averaged image with high-contrast conditions as described in Sect. 2.2.

2.5 Validity of the bar-pattern method

To verify the accuracy of the bar-pattern method, we compared the MTF values measured by the bar-pattern method and those measured by the conventional method using a wire phantom [23–25]. FBP images were used because its linearity was suitable for this comparison.

The wire phantom consisted of a cylindrical acrylic case with a diameter of 50 mm, in which a 0.05-mm thin tungsten wire was tensed along the center axis of the case. The case was filled with water. The wire phantom was placed along the isocenter line of CT system. The scanning conditions were 120 kV, 100 mA, 2.0 s/rot., and 80×0.5 mm detector configuration. CT images were reconstructed by FBP and four strengths of AIDR 3D with 50 mm DFOV, 0.5-mm slice thickness, and a reconstruction kernel of FC12. To extract a line spread function (LSF) from the wire CT image, we used the numerical slit scanning method proposed by Giger et al. [26]. The slit size ($x \times y$) was set to 1×40 pixels, and the scanning was performed in the x -direction. By application of slit scanning, an LSF with 256 data points was obtained, and the tail portion of the data on both sides far from the LSF center was replaced by zero data for reduction of the adverse influence of noise in the tail portions [27]. The MTF was calculated by use of the one-dimensional Fourier transform of the corrected LSF.

2.6 MTF of iterative reconstruction

1. We measured the MTFs of the FBP and two different strengths of AIDR 3D (weak and strong) from the averaged images of the bar-pattern phantom. The image number for the averaging was determined for the minimally required CNR that was already obtained in the investigation (see Sects. 2.4 and 3.1). To examine the dose dependence of the resolution property, we measured an MTF at a high-dose condition with a tube current of 270 mA. Thirty-two images for averaging were used each for FBP and AIDR 3D weak under the high-dose condition.

3 Results

3.1 Required CNR

Figure 4 shows the relationships between CNR and CTF error (difference from the true CTF value) and between

CNR and percentage error of the CTF, for 0.25, 0.5, and 1.0 cycles/mm. The CTF errors dropped at the CNR level of 24, and the errors were sufficiently small for CNR levels of 28 and above. Therefore, we determined the CNR level of 28 as the requisite for adequate accuracy of the MTF measurement using the bar-pattern method.

3.2 Validity of the bar-pattern method

Figure 5 shows MTF results for the wire and bar-pattern methods measured from the FBP images. For the bar-pattern method, the results of high- and middle-contrast conditions were indicated. The results of the bar-pattern method mostly agreed with those of the wire method; therefore, the accuracy of the bar-pattern method was validated.

3.3 MTF measured by the wire method

Figure 6 shows MTF results for the conventional wire method for FBP and four strengths of AIDR 3D. All MTF results were correctly identical, and this demonstrates that the resolution property for high-contrast objects was independent of the AIDR 3D strength.

3.4 MTF for AIDR 3D

Figure 7a shows MTF results for the middle-contrast condition for FBP; weak and strong of AIDR 3D. For the MTF plots of AIDR 3D, Gaussian-fitted MTF curves were also indicated. The frequencies at 10 % MTF for FBP, weak, and strong were 0.64, 0.56, and 0.44, respectively. The MTF of AIDR 3D decreased with the strength of AIDR 3D.

Figure 7b shows MTF results for FBP and weak strength of the noise reduction level of AIDR 3D for two different dose levels (270 and 80 mA). The volume computed tomography dose indices (CTDI_{vol}) for high- and low-dose levels were 44.2 and 11.5 mGy, respectively. The MTF of AIDR 3D varied depending on the dose level. The frequency at 10 % MTF decreased from 0.618 to 0.562 with a decrease in the dose level.

3.5 Processed images

Figure 8 shows bar-pattern images processed by the image-averaging technique for FBP, weak of AIDR 3D with high dose, weak of AIDR 3D with low dose, and strong of AIDR 3D with low dose. The CNR values of original images with low dose for FBP, high dose for weak of AIDR 3D, and low dose for weak and strong of AIDR 3D were 2.43, 4.67, 3.60, and 6.50, respectively. The sharpness of weak with high dose was almost equal to that of FBP. For the low

Fig. 4 Relationships **a** between CNR and CTF error and **b** between CNR and percentage error of CTF value

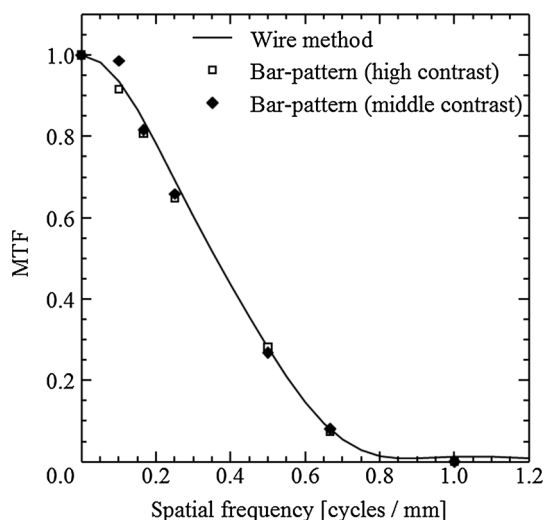
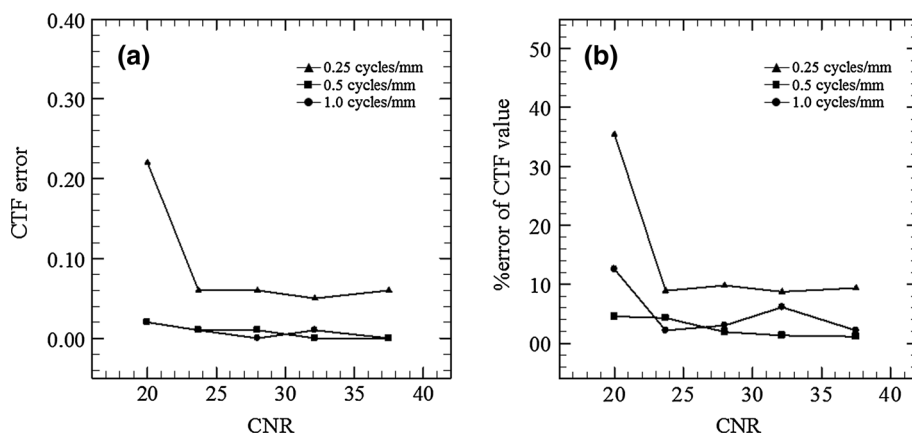


Fig. 5 MTF results for the wire and bar-pattern methods for FBP images

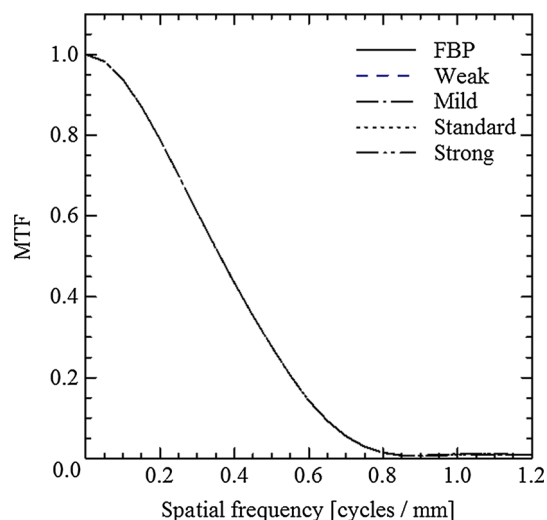


Fig. 6 MTF results for the conventional wire method for FBP and four strengths of AIDR 3D

dose, sharpness was degraded by the weak and strong of AIDR 3D, in which strong showed the lowest sharpness. Especially at 0.50- and 0.67-cycles/mm bar-pattern segments (areas within dotted line boxes in Fig. 8), the bar separation changes were remarkable. These findings were well correlated with the MTF results measured by the bar-pattern method.

4 Discussion

The results of the conventional wire method showed no difference in spatial resolution between FBP and AIDR 3D. Miéville et al. [12] presented the MTF results of three IRs, ASIR, VEO (GE Healthcare, Milwaukee, WI, USA) and iDose⁴ (Philips Healthcare, Cleveland, OH, USA) measured by use of a high-contrast bead object. In this work, ASIR and iDose⁴ provided almost the same MTF as that of

FBP, and VEO indicated a higher MTF than that of FBP. Gervaise et al. [8] demonstrated MTF results of the first generation of IR developed by Toshiba Medical Systems, AIDR, measured using a phantom including a 0.28-mm tungsten wire. In the study, there was no spatial resolution difference between FBP and AIDR. Because IRs are generally based on a non-linear process, these results are not more than those for high-contrast objects only. In addition, the conventional wire or bead methods require a small DFOV to provide accurate LSFs with sufficiently small sampling pitches [23–25]. Because it is possible that the IRs resolution depends on the DFOV, MTF results measured from wire or bead images do not indicate the correct MTF corresponding to clinical images with large DFOVs for adult bodies.

The image-averaging technique was effective for obtaining a sufficient CNR (28 and more) for a middle contrast of 50 HU. In the middle-contrast condition, the

Fig. 7 **a** MTF results for the middle-contrast condition for FBP; weak and strong AIDR 3D. For MTF plots of AIDR 3D, Gaussian-fitted MTF curves are also indicated. **b** MTF results for FBP and weak AIDR 3D for two different dose levels (44.2 and 11.5 mGy)

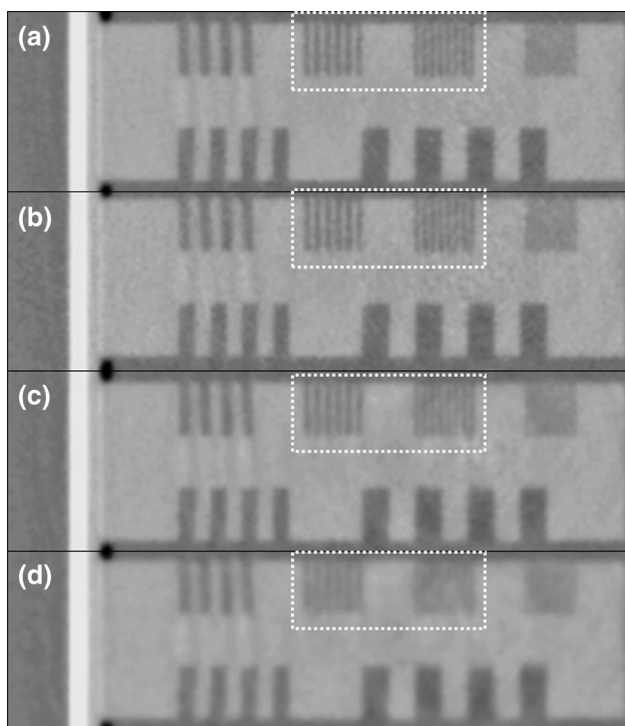
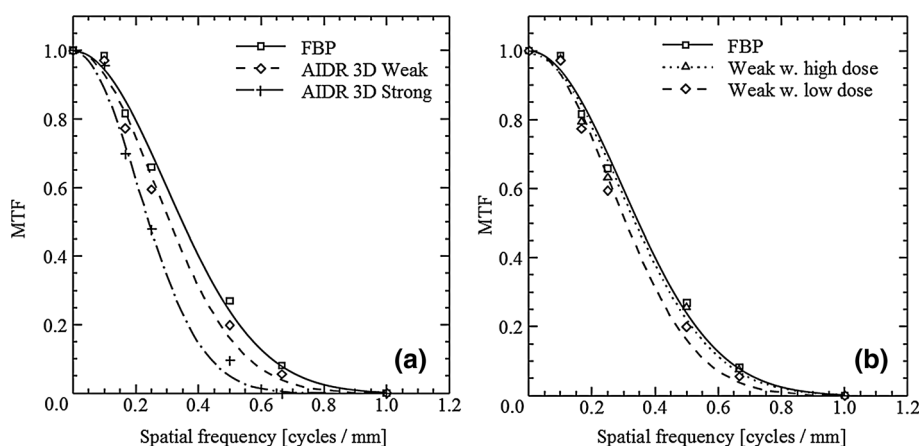


Fig. 8 Processed images for **a** FBP (11.5 mGy), **b** weak AIDR 3D with high dose (44.2 mGy), **c** weak AIDR 3D with low dose (11.5 mGy), **d** strong AIDR 3D with low dose (11.5 mGy). Especially at 0.50- and 0.67-cycles/mm bar-pattern segments (areas within dotted line boxes in Fig. 8), the bar separation changes were remarkable. The $CTDI_{vol}$ values for the images are shown in the brackets

image-averaging technique allows us to measure the spatial resolution with low noise. It was not difficult to repeat scans 50 times because the CT system used had a sufficient heat capacity for the X-ray tube. This level of heat capacity is not especially high; therefore, the image-averaging technique can be applied to most current CT systems. In addition, the tilted placement of the bar-pattern phantom used for obtaining a sufficiently small sampling pitch was

effective in the application with large DFOVs corresponding to clinical use.

The MTF results for FBP images obtained from both methods with the bar pattern and a wire were almost identical. Further, in the comparison study between the high- and middle-contrast conditions with the bar pattern, the MTFs of both the contrasts showed almost identical values. This demonstrates that the image-averaging technique applied to the middle-contrast images did not affect the MTF measurement accuracy, as shown in Fig. 5, because the alignment difference among images for the image-averaging could be ignored. In most MTF results for the bar pattern, MTF increases at 0.1 cycles/mm were found. Because the ring artifacts can be recognized at the segment with 5-mm bar (with a frequency of 0.1 cycles/mm) in Fig. 8, it was suspected that the MTF increases were caused by the artifact-related profile distortions. Although the image-averaging technique is effective in reducing the random noise (quantum noise), it does not work properly to reduce the ring artifact and other fixed pattern noises. Therefore, besides a measurement procedure that uses our method, more careful calibration operations, which were usually performed with air or water phantoms to reduce these artifacts, are required.

For the middle-contrast condition, the MTF of AIDR 3D decreased with the strength of the IR process compared with FBP. In the strategy of dose reduction by use of IRs, we hope that the IRs maintain the resolution while simultaneously reducing the noise for objects with any contrasts. However, AIDR 3D was not able to maintain the resolution for the middle-contrast objects which requires the resolution clinically. In addition, the MTF of AIDR 3D decreased under low-dose conditions, while the MTF was almost maintained with high-dose conditions. These results indicated that the more noise reduction we expect, the more resolution degradation occurs in IR images. Unfortunately, these relationships make it difficult to select the strength setting and the dose reduction rates by operators.

Our study has several limitations. First, because we measured MTFs at a fixed position of the bar-pattern phantom, in our results the effects of the directional or positional dependence of the resolution might be mixed. Second, in this study, we did not have a comparison with the method of Richard et al. [18] by use of cylindrical objects. Mori and Machida [28] proposed an MTF calculation method which can be used for edge images with CNRs as low as 2. Although it was thought that this method could be applied to IR images, we did not compare our method with their method. Thus, the shape dependence of the resolution was not investigated.

5 Conclusion

With our method, in which we used a combination of the bar-pattern phantom and the image-averaging technique, it was possible to evaluate the resolution of IR for the middle contrast (50 HU) with reasonable accuracy. The results obtained with our method clarified that the resolution of a tested IR was degraded with the strength of the IR process and dose reduction. In the determination process of the dose reduction rate by IRs, the contrast and dose dependencies of MTF, which can be evaluated accurately by our method, should be considered.

Conflict of interest The authors declare that they have no conflict of interest.

References

- Nishii T, Kono AK, Negi N, Hashimura H, Uotani K, Okita Y, Sugimura K. The feasibility of a 64-slice MDCT for detection of the Adamkiewicz artery: comparison of the detection rate of intravenous injection CT angiography using a 64-slice MDCT versus intra-arterial and intravenous injection CT angiography using a 16-slice MDCT. *Int J Cardiovasc Imaging*. 2013;29:127–33.
- Hurlock GS, Higashino H, Mochizuki T. History of cardiac computed tomography: single to 320-detector row multislice computed tomography. *Int J Cardiovasc Imaging*. 2009;25:31–42.
- Komissarova M, Chong S, Frey K, Sundaram B. Imaging of acute pulmonary embolism. *Emerg Radiol*. 2013;20:89–101.
- Brenner DJ, Hall EJ. Computed tomography—an increasing source of radiation exposure. *New Engl J Med*. 2007;357:2277–84.
- Fleischmann D, Boas FE. Computed tomography—old ideas and new technology. *Eur Radiol*. 2011;21:510–7.
- Hara AK, Paden RG, Silva AC, Kujak JL, Lawder HJ, Pavlicek W. Iterative reconstruction technique for reducing body radiation dose at CT: feasibility study. *Am J Roentgenol*. 2009;193:764–71.
- Singh S, Kalra MK, Hsieh J, Licato PE, Do S, Pien HH, Blake MA. Abdominal CT: comparison of adaptive statistical iterative and filtered back projection reconstruction techniques. *Radiology*. 2010;257:373–83.
- Gervaise A, Osemont B, Lecocq S, Noel A, Micard E, Felblinger J, Blum A. CT image quality improvement using adaptive iterative dose reduction with wide-volume acquisition on 320-detector CT. *Eur Radiol*. 2012;22:295–301.
- Irwan B, Nakanishi S, Blum A (2012) AIDR 3D—reduces dose and simultaneously improves image quality. Toshiba Medical Systems Whitepaper. Available via http://www.toshiba-medical.eu/upload/TMSE_CT/White%20Papers/White%20Papers/Toshiba_White%20paper%20CT_nov11.pdf?epslanguage=en. Accessed Oct 2012.
- Willemink MJ, de Jong PA, Leiner T, de Heer LM, Nievelstein RA, Budde RP, Schilham AM. Iterative reconstruction techniques for computed tomography part 1: technical principles. *Eur Radiol*. 2013;23:1623–31.
- American Association of Physicists in Medicine. Diagnostic Radiology Committee. Task Force on CT Scanner Phantoms. In: Judy PF (eds) Phantoms for performance evaluation and quality assurance of CT scanners. American Association of Physicists in Medicine. 1977.
- Miéville FA, Gudinchet F, Brunelle F, Bochud FO, Verdun FR. Iterative reconstruction methods in two different MDCT scanners: physical metrics and 4-alternative forced-choice detectability experiments—A phantom approach. *Phys Medica*. 2013;29:99–110.
- Suess C, Kalender WA, Coman JM. New low-contrast resolution phantoms for computed tomography. *Med Phys*. 1999;26:296–302.
- Berber E, Foroutani A, Garland AM, Rogers SJ, Engle KL, Ryan TL, Siperstein AE. Use of CT Hounsfield unit density to identify ablated tumor after laparoscopic radiofrequency ablation of hepatic tumors. *Surg Endosc*. 2000;14:799–804.
- Funama Y, Awai K, Nakayama Y, Kakei K, Nagasue N, Shimamura M, Yamashita Y. Radiation dose reduction without degradation of low-contrast detectability at abdominal multislice CT with a low-tube voltage technique: phantom study 1. *Radiology*. 2005;237:905–10.
- Pohle K, Achenbach S, MacNeill B, Ropers D, Ferencik M, Moselewski F, Daniel WG. Characterization of non-calcified coronary atherosclerotic plaque by multi-detector row CT: comparison to IVUS. *Atherosclerosis*. 2007;190:174–80.
- Cham MD, Yankelevitz DF, Shaham D, Shah AA, Sherman L, Lewis A, Henschke CI. Deep venous thrombosis: detection by using indirect CT Venography1. *Radiology*. 2000;216:744–51.
- Richard S, Husarik DB, Yadava G, Murphy SN, Samei E. Towards task-based assessment of CT performance: system and object MTF across different reconstruction algorithms. *Med Phys*. 2012;39:4115–22.
- Fujita H, Tsai DY, Itoh T, Morishita J, Ueda K, Ohtsuka A. A simple method for determining the modulation transfer function in digital radiography. *IEEE Trans Med Imaging*. 1992;11:34–9.
- Stierstorfer K, Spahn M. Self-normalizing method to measure the detective quantum efficiency of a wide range of x-ray detectors. *Med Phys*. 1999;26:1312–9.
- Cunningham IA, Fenster A. A method for modulation transfer function determination from edge profiles with correction for finite-element differentiation. *Med Phys*. 1987;14:533–7.
- Gupta AK, Nelson RC, Johnson GA, Paulson EK, Delong DM, Yoshizumi TT. Optimization of eight-element multi-detector row helical CT technology for evaluation of the Abdomen1. *Radiology*. 2003;227:739–45.
- Boedeker KL, Cooper VN, McNitt-Gray MF. Application of the noise power spectrum in modern diagnostic MDCT: part I. Measurement of noise power spectra and noise equivalent quanta. *Phys Med Biol*. 2007;52:4027–46.
- Nickoloff EL. Measurement of the PSF for a CT scanner: appropriate wire diameter and pixel size. *Phys Med Biol*. 1988;33:149–55.
- Boone JM. Determination of the presampled MTF in computed tomography. *Med Phys*. 2001;28:356–60.

-
26. Giger ML, Doi K, Fujita H. Investigation of basic imaging properties in digital radiography. 7. Noise Wiener spectra of II-TV digital imaging systems. *Med Phys.* 1986;13:131–8.
 27. Bischof CJ, Ehrhardt JC. Modulation transfer function of the EMI CT head scanner. *Med Phys.* 1977;4:163–7.
 28. Mori I, Machida Y. Deriving the modulation transfer function of CT from extremely noisy edge profiles. *Radiol Phys Technol.* 2009;2(1):22–32.